

Synergistic Flame Retardant Effect of Organic Boron Flame Retardant and Aluminum Hydroxide on Polyethylene

Lianghui Ai, Shanshan Chen, Liu Yang, and Ping Liu*

State Key Laboratory of Luminescent Materials and Devices, Research Institute of Materials Science,
South China University of Technology, Guangzhou 510640, China

(Received December 20, 2019; Revised April 3, 2020; Accepted April 24, 2020)

Abstract: This study aimed to develop an organic/inorganic synergistic flame retardant on polyethylene (PE). Hexakis-(4-boronic acid-phenoxy)-cyclophosphazene (CP-6B) was used as organic flame retardant to improve the flame retardant efficiency of aluminum hydroxide (ATH) on PE. The limiting oxygen index (LOI) value of PE/20 %ATH/20 %CP-6B reached 27.0 %, and vertical burning (UL 94) V-0 rating was attained. The peak heat release rate (*pk-HRR*) of PE/20 %ATH/20 %CP-6B was 33.7 % and 75.5 % of pure PE and PE/40 %ATH, respectively. The flame retardant mechanism of PE composites was also investigated using scanning electron microscopy (SEM), energy dispersive X-ray (EDX), X-ray diffraction (XRD), muffle furnace, Fourier transform infrared (FTIR), and Pyrolysis-gas chromatography-mass spectrometry (PY-GC-MS). The results showed that ATH/CP-6B was an efficient flame retardant, which was effective in the gas phase and condensed phase simultaneously. CP-6B improved the flame retardant efficiency of PE/ATH and reduced the effect of ATH on the mechanical properties of PE.

Keywords: Organic boron, Aluminum hydroxide, Synergistic effect, Polyethylene

Introduction

Polyethylene (PE) is a crucial thermoplastic material that has diverse applications [1-3]. Since low-density polyethylene (LDPE) exhibits good toughness, electrical insulation properties, chemical resistance, easy processability, and low cost, PE is widely used in various industries, such as wire and cable industry [4-8]. However, PE is easily flammable and dripping, which brings fire risk during application [9-14]. The use of flame retardants to improve the flame retardancy of PE is critical to its application [15-18]. Halogen-based flame retardants are easy to migrate and bioaccumulation, and easily release large amounts of smoke and toxic corrosive substances during burning [19-26].

The aluminum hydroxide (ATH) is an environment-friendly inorganic flame retardant. In addition, ATH is abundant and cheap [27-33]. However, in order to achieve higher flame retardancy, the addition of ATH usually needs to exceed 50 %, which makes it poorly compatible with the substrate and affects the mechanical properties of the substrate [34-38]. Therefore, ATH is used in combination with other flame retardants [39-43].

During combustion, organic phosphorus flame retardants decompose to catalyze the dehydration and carbonization of the polymer to form a protective carbon layer with high heat resistance [44-46]. Organic nitrogen flame retardants decompose to produce a large number of noncombustible gases, which dilute combustible volatiles [47-49]. In general, in order to improve the flame retardant efficiency, the flame retardant contains a variety of flame retardant elements, of which more research on phosphorus and nitrogen flame retardants

[50-54]. Organic boron flame retardant can form a vitreous coating, reduce the temperature of the condensed phase, and isolate the volatile fuel [55-58]. There are few reports on the combination of organic boron flame retardants and ATH. In this paper, using hexakis-(4-boronic acid-phenoxy)-cyclophosphazene (CP-6B) as organic flame retardant and ATH as inorganic flame retardant, the synergistic flame retardant effect of CP-6B/ATH on PE was investigated. In addition, the mechanism was also investigated.

Experimental

Materials

PE (LDPE, F410-1) with a melt flow index of 5 g/10 min and density of 0.92 g/m³ was purchased from Shunlong Plastic Materials Co., Ltd. (Dongguan, China). ATH was obtained from Sinopharm Chemical Reagent Co., Ltd.

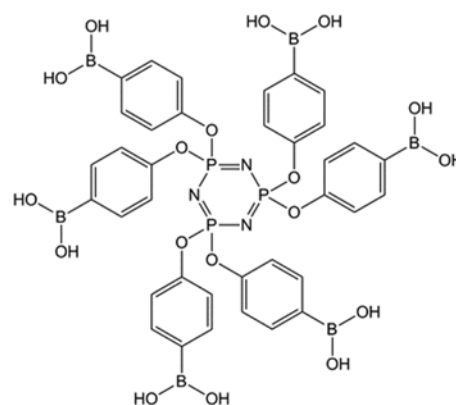


Figure 1. Structure of CP-6B.

*Corresponding author: mcpliu@scut.edu.cn

(Shanghai, China). CP-6B was synthesised in our laboratory, and the structure of CP-6B was shown in Figure 1 [55].

Characterization

Thermogravimetry (TG) analysis was tested using a Netzsch 209 F3 thermal analyzer with a nitrogen flow rate of 50 mL/min and a heating rate of 10 °C/min.

The LOI values were tested using a FTT oxygen index tester (ASTM D2863, 80×10×4 mm³). Vertical burning (UL 94) was tested using a FTT vertical burning tester (ASTM 3801, 125×12.7×3.2 mm³), and the burning grades were divided into NR, V-2, V-1, and V-0. Cone calorimeter tests were tested using a FTT cone calorimeter (ISO-5660, 100×100×3 mm³), and the incident flux was 50 kW/m².

The SEM morphology of the residual chars was tested using an EVO18 scanning electron microscopy. Elemental analysis of the residual chars was tested using an EVO18 energy dispersive X-ray. FTIR was recorded using a Nicolet 6700 FTIR spectrometer. XRD was analyzed using an X'Pert Pro X-ray diffractometer. PY-GC-MS was recorded using a GCMS-QP2010 plus pyrolysis-gas chromatography mass spectrometer.

The tensile strength was measured with an AG-Xplus electronic universal testing machine. The testing speed was 5 mm/min, and the sample dimensions were 150×10×4 mm³. The flexural strength was measured with an AGS-10KNI universal electronic tensile testing machine. The testing speed was 20 mm/min, and the sample dimensions were 80×10×4 mm³.

Table 1. Weight ratios of PE samples

Sample	PE (g)	ATH (g)	CP-6B (g)
PE	100	0	0
PE/5 %CP-6B	95	0	5
PE/10 %CP-6B	90	0	10
PE/20 %CP-6B	80	0	20
PE/10 %ATH	90	10	0
PE/20 %ATH	80	20	0
PE/30 %ATH	70	30	0
PE/40 %ATH	60	40	0
PE/30 %ATH/10 %CP-6B	60	30	10
PE/20 %ATH/20 %CP-6B	60	20	20

Preparation of PE Samples

PE, ATH, and CP-6B were melt-mixed in a twin-roller mill at 115 °C for 10 min, and the roller speed was 60 rpm. The samples were hot-pressed at 145 °C for 15 min into sheets. The sheet was cut into the required dimensions for testing. The samples are listed in Table 1.

Results and Discussion

Thermogravimetry (TG) and Differential Thermogravimetry (DTG) Analyses

Figure 2 shows the TG and DTG curves of the PE samples. The characteristic thermal decomposition data are

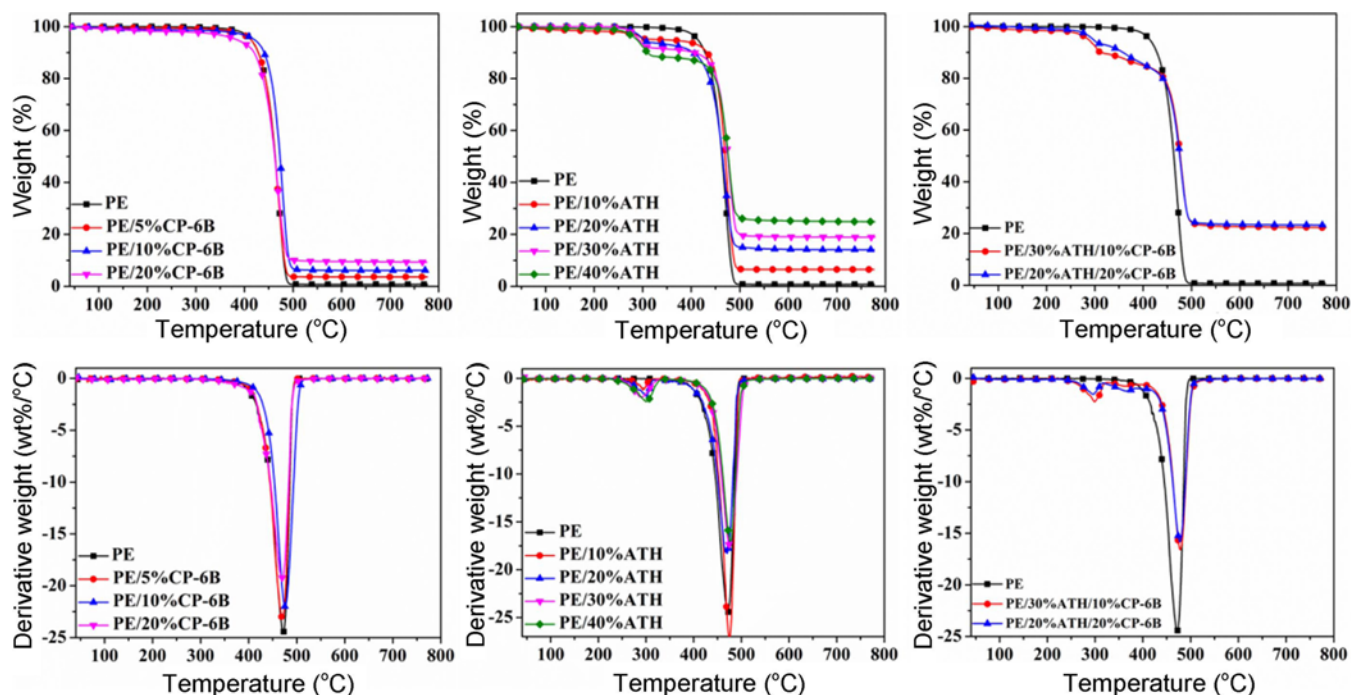


Figure 2. TG and DTG curves for PE samples.

Table 2. Thermal decomposition characteristics of PE samples

Sample	T_{onset}^a (°C)	T_{max1}^b (°C)	T_{max2} (°C)	T_{max3} (°C)	W_{800}^c (%)
PE	413.5	472.8	-	-	0.7
PE/5 %CP-6B	413.3	471.2	-	-	3.6
PE/10 %CP-6B	407.3	472.1	-	-	6.2
PE/20 %CP-6B	383.9	468.1	-	-	9.3
PE/10 %ATH	333.0	293.4	475.4	-	6.5
PE/20 %ATH	302.4	301.0	470.3	-	14.1
PE/30 %ATH	292.0	297.3	480.9	-	18.9
PE/40 %ATH	287.9	294.2	478.9	-	24.9
PE/30 %ATH/10 %CP-6B	287.0	302.8	364.6	479.1	22.4
PE/20 %ATH/20 %CP-6B	293.6	298.9	368.6	478.7	23.3

^aInitial temperature at 5 % mass loss, ^btemperature at the maximum mass loss rate, and ^cresidual char yield at 800 °C.

summarized in Table 2. PE is a thermoplastic resin containing only C and H and exhibits poor flame retardancy. Pure PE was almost completely decomposed, and its residual char yield at 800 °C was only 0.7 %. When CP-6B was added, the weight loss stage of PE/CP-6B was basically the same as that of pure PE, and there was only one weight loss peak. However, the residual char yield at 800 °C of PE/CP-6B improved. The residual char yield at 800 °C of PE/20 %CP-6B was 9.3 %, the increased in residual char yield arose from undecomposed fragments of CP-6B. When ATH was added, PE/ATH exhibited two weight loss stages. The first peak was the decomposition of ATH, and the second peak was the decomposition of PE. ATH decomposed to form Al_2O_3 , and the char layer containing Al_2O_3 could protect internal PE. The residual char yield of PE/ATH was higher than that of pure PE and PE/CP-6B due to the large amount of Al_2O_3 .

When ATH and CP-6B were added together, PE/ATH/CP-6B exhibited three weight loss peaks. The first peak was in the temperature range of 260-320 °C, which was the decomposition of ATH to generate Al_2O_3 . The second peak at 320-380 °C was only detected in PE/ATH/CP-6B. CP-6B was catalytically decomposed to form B-O-C char due to the presence of Al_2O_3 . The third peak corresponded to the decomposition of PE. The ATH/CP-6B formed a char layer to protect PE from further decomposition, and the residual char yield of PE/20 %ATH/20 %CP-6B reached 23.3 %.

LOI and UL 94

Table 3 shows the LOI value and UL 94 rating of the PE samples. When adding 10 wt.% CP-6B, the LOI value of the PE only increased from 17.7 % to 21.7 %, and PE/10 %CP-6B did not pass the UL 94 rating test. PE was composed of a simple alkyl chain without any flame retardant properties. When the amount of the flame retardant was low, the

Table 3. LOI value and UL 94 data of PE samples

Sample	LOI (%)	ΔLOI (%)	UL-94 (3.2 mm) ^a	Dripping
PE	17.7±0.2	-	NR	Yes
PE/5 %CP-6B	19.8±0.2	2.1	NR	Yes
PE/10 %CP-6B	21.7±0.2	3.0	NR	Yes
PE/20 %CP-6B	24.0±0.2	6.3	V-2	Yes
PE/10 %ATH	18.7±0.2	1.0	NR	Yes
PE/20 %ATH	20.2±0.2	2.5	NR	Yes
PE/30 %ATH	23.4±0.2	5.7	NR	Yes
PE/40 %ATH	25.1±0.2	7.4	V-1	No
PE/30 %ATH/10 %CP-6B	25.5±0.2	7.8	V-0	No
PE/20 %ATH/20 %CP-6B	27.0±0.2	9.3	V-0	No

^aNR=no rating and $\Delta LOI=LOI-LOI$ (pure PE).

increase in the flame retardancy of PE limited. When the addition of CP-6B reached 20 wt.%, the LOI value of the PE increased from 17.7 % to 24.0 %, and PE/20 %CP-6B reached the UL 94 V-2 rating. The decomposition of CP-6B formed a char layer and produced nonflammable gas, which isolated internal resin and inhibited combustion heat.

When 10 wt.%, 20 wt.%, and 30 wt.% ATH were added, the LOI value of PE increased by 1.0 %, 2.5 %, and 5.7 %, respectively. When adding 40 wt.% ATH, the LOI value of the PE increased from 17.7 % to 25.1 %. PE/40 %ATH reached the UL 94 V-1 rating. The Al_2O_3 protective layer formed by physical accumulation was prone to cracks, resulting in reduced the oxygen isolation and heat insulation efficiency. Therefore, when ATH was added separately, a high amount of addition required. PE/ATH/CP-6B exhibited good flame retardant properties. The LOI value of PE/20 %ATH/20 %CP-6B reached 27.0 %, and the UL 94 combustion grade reached V-0 rating without dripping. The Al_2O_3 catalyzed the decomposition of CP-6B to form char layer. The heat resistant char layer prevented dripping. The ATH/CP-6B achieved higher flame retardant efficiency.

Cone Calorimeter Tests

Cone calorimeter tests can be used to evaluate the fire behavior of substrates. The relevant combustion data included peak heat release rate ($pk-HRR$), total heat release (THR), average rate of heat emission ($ARHE$), total oxygen consumption (TOC), mass loss, average effective heat combustion ($av-EHC$), and fire growth index (FGI). The results for PE samples are displayed in Figure 3 and Table 4.

The EHC reflects the combustion intensity of the released fuel. The $av-EHC$ of PE/ATH/CP-6B was lower than PE/ATH. The nonflammable gases produced by the decomposition of CP-6B diluted the volatile fuel and reduced the EHC . FGI can evaluate the fire hazard of a material. The FGI values of PE/20 %CP-6B and PE/40 %ATH were 79.9 % and 97.1 %

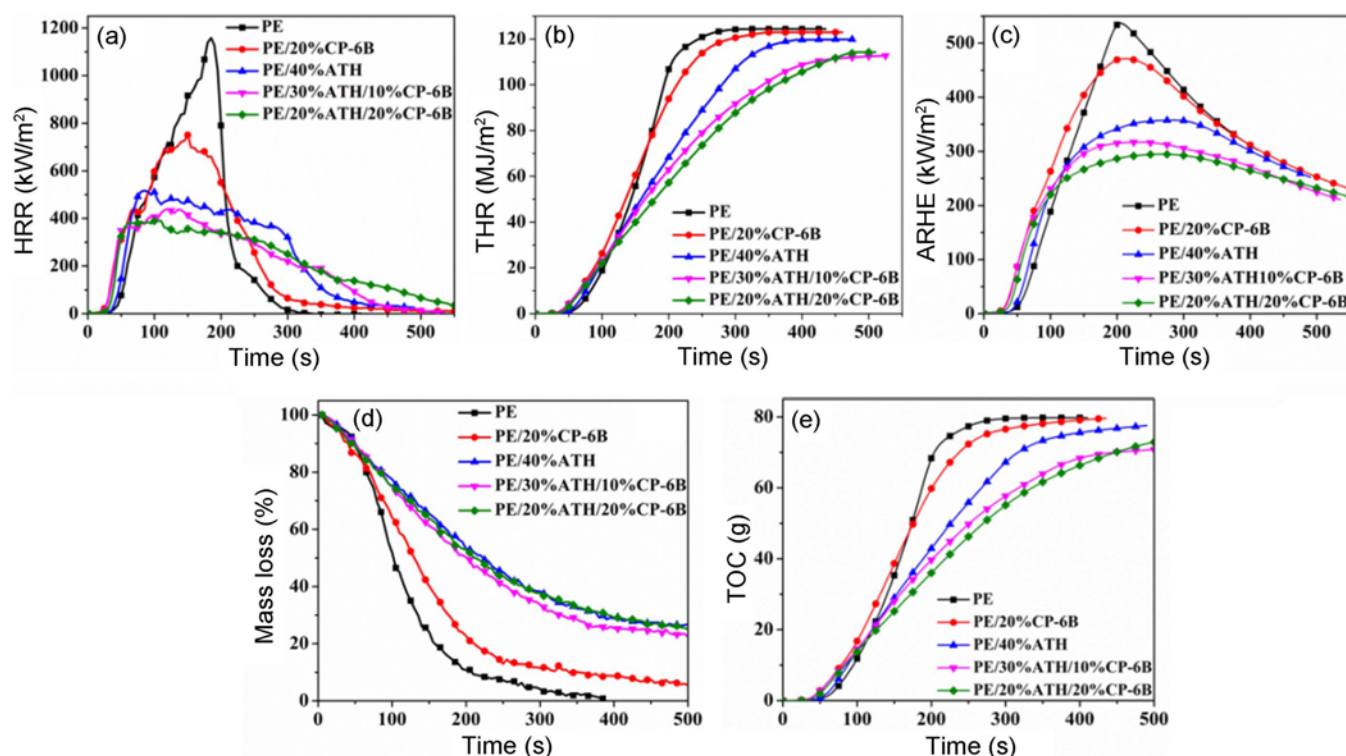


Figure 3. Cone calorimeter curves of PE samples; (a) *HRR*, (b) *THR*, (c) *ARHE*, (d) mass loss, and (e) *TOC*.

Table 4. Cone calorimeter data of PE samples

Sample	<i>pk-HRR</i> (kW/m ²)	<i>THR</i> (MJ/m ²)	<i>av-EHC</i> (MJ/kg)	<i>FGI</i> kW/(m ² ·K)	Residual char yield (%)
PE	1159±22	125±2	43.5±0.3	6.26	0.6
PE/20 %CP-6B	750±19	122±3	39.1±0.3	5.00	5.1
PE/40 %ATH	517±17	119±3	35.1±0.3	6.08	25.7
PE/30 %ATH/10 %CP-6B	440±18	112±2	31.2±0.3	3.67	23.1
PE/20 %ATH/20 %CP-6B	390±19	114±2	31.0±0.3	3.55	25.2

of those of pure PE, respectively. The *FGI* values of PE/20 %CP-6B was lower than that of PE/40 %ATH because CP-6B had simultaneous gas and condensed phase flame retardant mechanisms [54,55]. When 20 wt.% ATH and 20 wt.% CP-6B were added together, the *FGI* of PE/20 %ATH/20 %CP-6B was only about 56.7 % of that of pure PE, indicating that ATH/CP-6B effectively decreased the combustion intensity of PE and controlled the spread of fire.

The *pk-HRR* values of pure PE was 1159 kW/m², and the *THR* values of pure PE was 125 MJ/m². The *HRR* and *THR* values of PE/ATH/CP-6B were lower than PE/CP-6B and PE/ATH. The trend of *ARHE* was consistent with *HRR* and *THR*, indicating that adding CP-6B improved the flame retardant efficiency of ATH and reduced the release of combustion heat of PE. The residual char yield of pure PE was 0.6 %. When 40 wt.% ATH was added, the decomposition of PE became slower, and the residual char yield of PE/40 %

ATH reached 25.7 %. This finding could be due to the large amount of ATH decomposed to produce Al₂O₃. However, Al₂O₃ was physical accumulation, which was easy to crack, and the effect of heat insulation and oxygen isolation was poor. When 20 wt.% ATH and 20 wt.% CP-6B were added simultaneously, the mass loss rate of PE was further reduced, and the residual char yield of PE/20 %ATH/20 %CP-6B reached 25.2 %. Compared with PE/40 %ATH, the residual char yield of PE/20 %ATH/20 %CP-6B was almost the same. However the flame retardant efficiency improved. These results indicated that ATH/CP-6B inhibited the decomposition of PE.

TOC indicated the total oxygen mass consumed by the material during the cone calorimeter test. The *TOC* of pure PE was the largest, indicating the sufficient combustion of PE, the large amount of heat released by combustion, and the high risk of pure PE in fire. When 40 wt.% ATH was added,

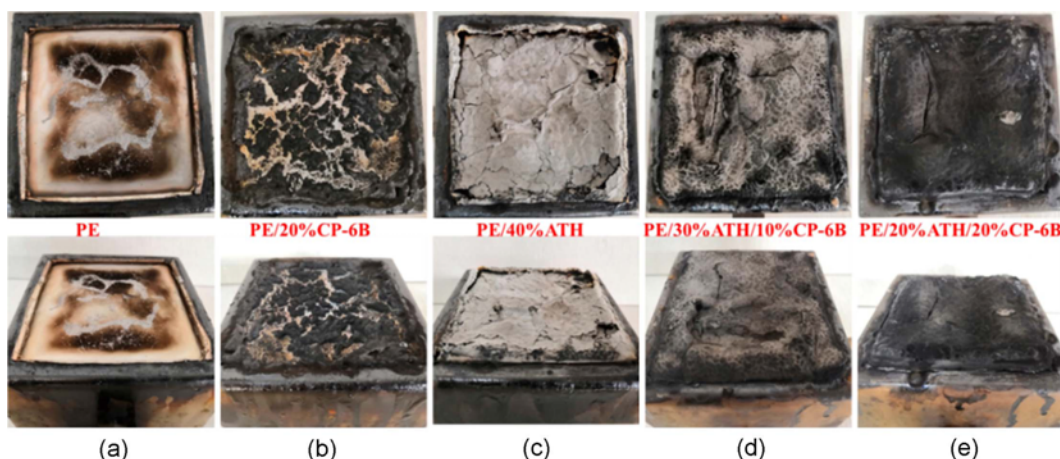


Figure 4. Photographs of residual chars from (a) pure PE, (b) PE/20 %CP-6B, (c) PE/40 %ATH, (d) PE/30 %ATH/10 %CP-6B, and (e) PE/20 %ATH/20 %CP-6B.

the *TOC* of PE decreased, indicating that the Al_2O_3 layer isolated oxygen. The *TOC* of PE/20 %ATH/20 %CP-6B and PE/30 %ATH/10 %CP-6B was lower than that of PE/40 %ATH. The decomposition of ATH and CP-6B released noncombustible gases and formed a carbon layer. Noncombustible gases diluted the volatile fuel, and the carbon layer also isolated oxygen to protect internal resin. These results indicated that CP-6B improved the flame retardant efficiency of ATH.

Figure 4 shows the photographs of the residual chars after the cone calorimeter tests. Pure PE consisted of alkyl chains and was extremely flammable. The residual char yield of PE/20 %CP-6B was low due to the low content of the charring agent. When 40 wt.% was added, although residual char of PE/40 %ATH contained a large amount of Al_2O_3 , many cracks were formed in the Al_2O_3 layer by physical

accumulation. However, with the addition of CP-6B, the effect of the carbon layer was improved. The residual char of PE/20 %ATH/20 %CP-6B was dense and continuous, and the char layer inhibited the decomposition of internal PE. This finding indicated that ATH/CP-6B was active in the condensed phase.

SEM

Figure 5 shows the SEM images of the residual of the PE samples after cone calorimeter tests. The residual char of PE/20 %CP-6B contained many holes and fragments. The residual char of PE/40 %ATH was not continuous and contained a large amount of Al_2O_3 powder. The residual char of PE/20 %CP-6B and PE/40 %ATH had poor protective effect on PE. However, when ATH and CP-6B were added together, the residual char of PE/ATH/CP-6B was dense and

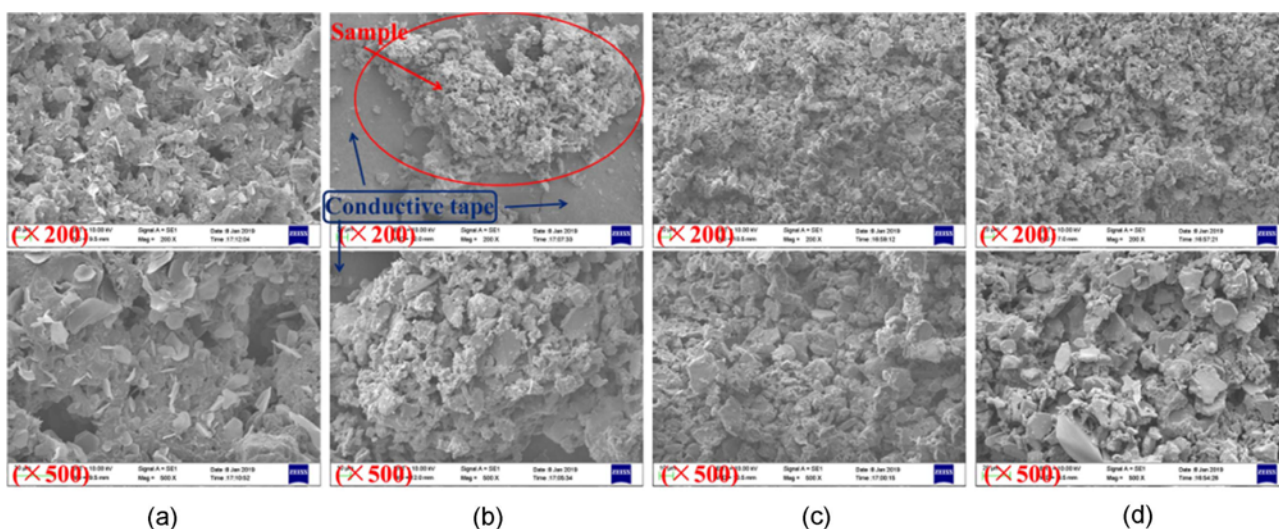


Figure 5. SEM images of residual chars from (a) PE/20 %CP-6B, (b) PE/40 %ATH, (c) PE/30 %ATH/10 %CP-6B, and (d) PE/20 %ATH/20 %CP-6B.

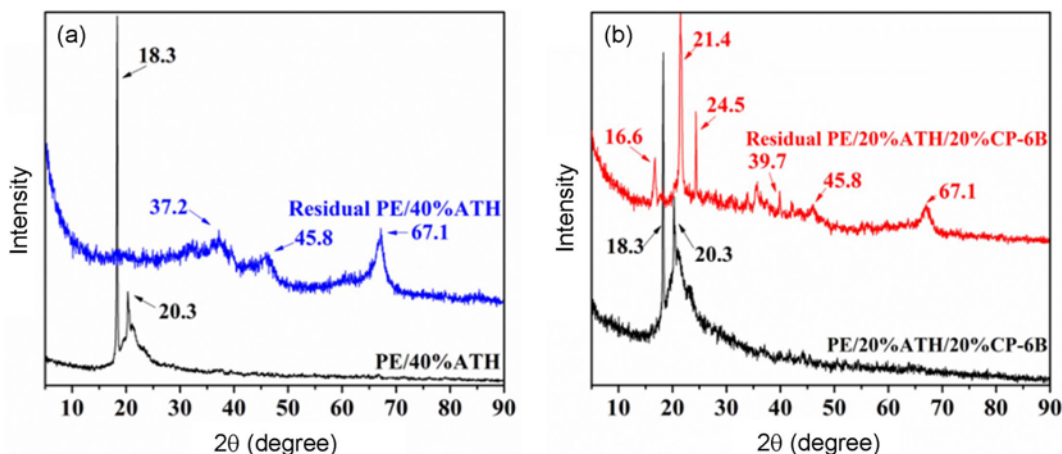


Figure 6. XRD patterns of residual samples, (a) PE/40 %ATH and (b) PE/20 %ATH/20 %CP-6B.

compact. The dense carbon layer played a protective role by isolating internal resin and preventing heat exchange. The addition of CP-6B increased the integrity of the char and it became continuous form with stable character. Accordingly, the barrier effect of char increased. Thus the condensed phase action of ATH increased.

XRD

Figure 6 shows the XRD pattern of the residual chars of PE/40 %ATH and PE/20 %ATH/20 %CP-6B. PE/40 %ATH and PE/20 %ATH/20 %CP-6B samples had two diffraction peaks at $2\theta = 18.3^\circ$ and 20.3° , because they both contained ATH. The residual char of PE/40 %ATH and PE/20 %ATH/20 %CP-6B exhibited diffraction peaks at $2\theta = 37.2^\circ$, 39.7° , 45.8° , and 67.1° , which corresponded to Al_2O_3 . The residual char of PE/20 %ATH/20 %CP-6B exhibited diffraction peaks at $2\theta = 24.5^\circ$, corresponding to BPO_4 , and at $2\theta = 16.6^\circ$ and 21.4° , corresponding to AlPO_4 . PE/20 %ATH/20 %CP-6B decomposed to form stable carbon layers containing Al_2O_3 , BPO_4 , and AlPO_4 . The formed protective layer containing Al and P protected the internal resin from further oxidative decomposition.

Elemental Analysis

Elemental analysis of the residual chars is shown in Table 5. Pure PE was decomposed completely without elemental analysis test results. PE/20 %CP-6B showed higher carbon, oxygen, and phosphorus contents than pure PE. CP-6B decomposed to form a carbon layer containing phosphorus, oxygen, and carbon. PE/40 %ATH showed higher aluminum and oxygen contents due to the presence of Al_2O_3 . PE/30 %ATH/10 %CP-6B and PE/20 %ATH/20 %CP-6B contained phosphorus and aluminum. These results indicated that the carbon layer contained phosphorus, oxygen, and aluminum. The heat-resistant and oxidation-resistant char layer protected the internal resin from further oxidative decomposition.

Table 5. Elemental analysis of the residual char

Sample	Elemental composition (wt.%)			
	C	O	P	Al
PE	-	-	-	-
PE/20 %CP-6B	19.98	60.64	19.38	0
PE/40 %ATH	16.42	50.95	0	32.64
PE/30 %ATH/10 %CP-6B	15.29	47.46	1.10	36.15
PE/20 %ATH/20 %CP-6B	12.38	49.47	4.91	33.25

Morphologies of PE Samples at Different Temperatures

Figure 7 shows the photographs of PE samples stored in a muffle furnace at various temperatures for 15 min. Pure PE began to melt at 150°C , and discoloration occurred at 300°C , indicating that the material started to decompose. No residual carbon was found in the crucible. PE/20 %CP-6B produced bubbles at 150°C , expanded at 250°C , and still had carbon residues at 650°C . PE/40 %ATH melted slightly at 250°C , and discoloration occurred 300°C . PE/40 %ATH had higher thermal stability than pure PE and large amount of Al_2O_3 residue at 650°C . The change trend of PE/30 %ATH/10 %CP-6B was almost the same as that of PE/20 %CP-6B. PE/30 %ATH/10 %CP-6B produced a large amount of white powder at 650°C , which might be Al_2O_3 . By contrast, PE/20 %ATH/20 %CP-6B started to expand at 350°C , and a large amount of residual carbon formed at 650°C . PE/20 %ATH/20 %CP-6B had the best heat resistance and exhibited better flame retardant properties. These phenomena indicated that CP-6B improved the heat resistance and flame retardant efficiency of PE/ATH.

FTIR

Figure 8 shows the FTIR spectra of PE/40 %ATH and PE/20 %ATH/20 %CP-6B residual char. The residual char of PE/40 %ATH and PE/20 %ATH/20 %CP-6B still had absorption

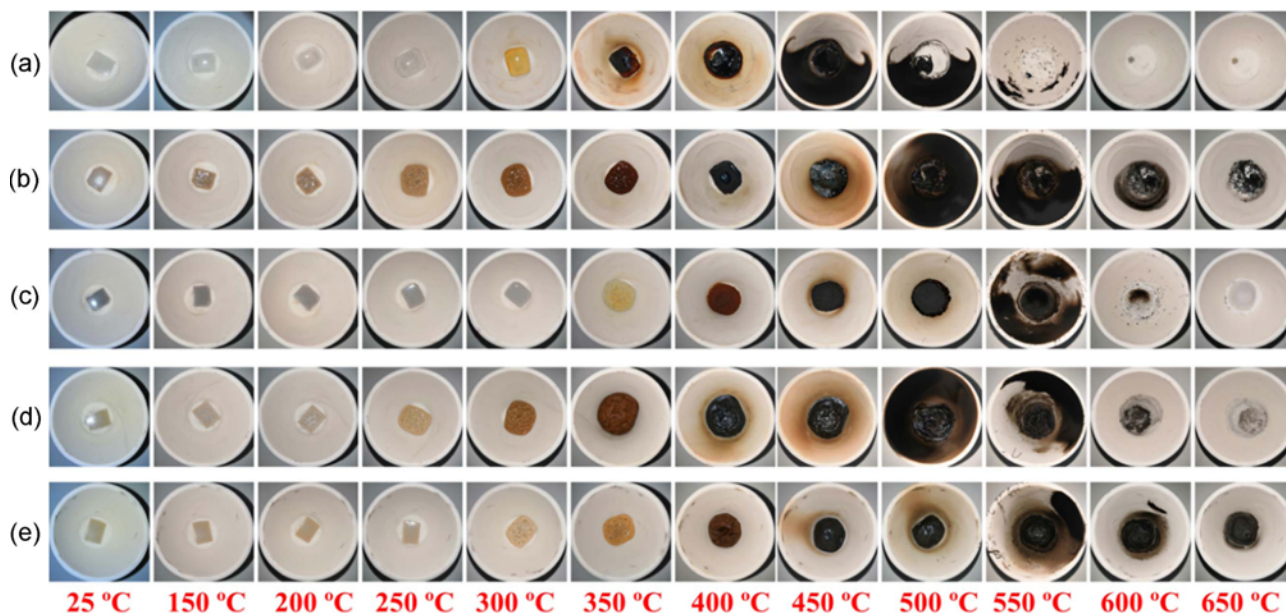


Figure 7. Photographs of PE samples at different temperatures; (a) PE, (b) PE/20 %CP-6B, (c) PE/40 %ATH, (d) PE/30 %ATH/10 %CP-6B, and (e) PE/20 %ATH/20 %CP-6B.

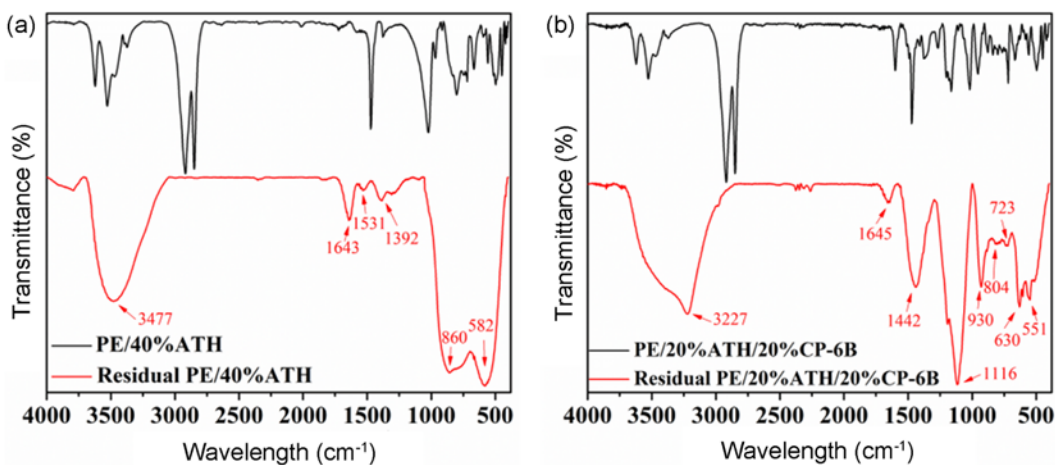


Figure 8. FTIR spectra of residual char (a) PE/40 %ATH and (b) PE/20 %ATH/20 %CP-6B.

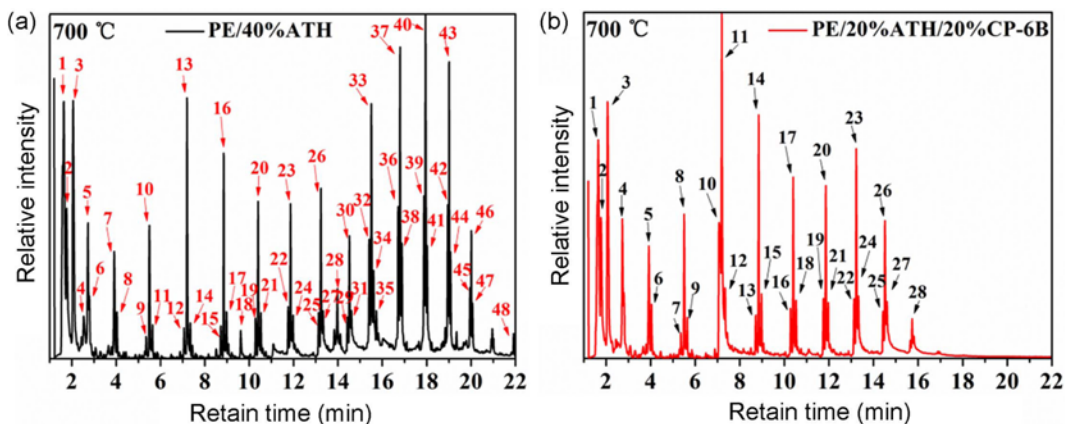


Figure 9. PY-GC-MS of PE/40 %ATH (a) and PE/20 %ATH/20 %CP-6B (b) at 700 °C.

Table 6. Peaks structure of PE/40 %ATH volatiles

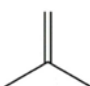


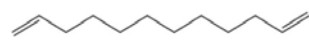



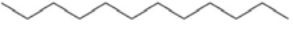
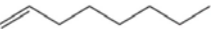
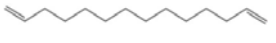
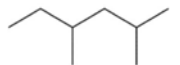




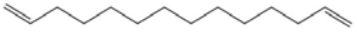


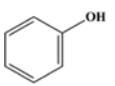

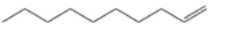
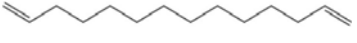
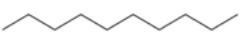


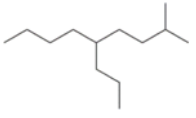
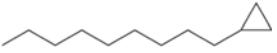
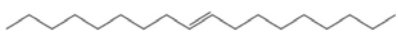
Peak	m/z	Structure	Peak	m/z	Structure
1	56		25	194	
2	70		26	182	
3	84		27	212	
4	78		28	224	
5	98		29	194	
6	100		30	252	
7	112		31	184	
8	114		32	194	
9	124		33	280	
10	126		34	226	
11	156		35	266	
12	138		36	222	
13	140		37	238	
14	142		38	240	
15	152		39	194	
16	168		40	252	
17	156		41	254	
18	210		42	194	
19	166		43	266	
20	168		44	296	
21	170		45	278	
22	194		46	322	
23	182		47	184	
24	212		48	296	

peaks, which revealed that some structures retained after the decomposition of PE/40 %ATH and PE/20 %ATH/20 %CP-6B. The residual char of PE/20 %ATH/20 %CP-6B had more infrared absorption peaks than the residual char of PE/40 %ATH, indicating the better thermal stability and flame retardancy of PE/20 %ATH/20 %CP-6B than that of PE/40 %ATH. ATH/CP-6B formed a stable carbon layer and decomposed to release a large amount of nonflammable gas, thereby improving the flame retardancy of materials by diluting flammable volatile substances.

PY-GC-MS

Figure 9 is the PY-GC-MS curves of PE/40 %ATH (a) and PE/20 %ATH/20 %CP-6B (b) at 700 °C. Table 6 lists the peaks structure of PE/40 %ATH volatiles, and Table 7 lists the peaks structure of PE/20 %ATH/20 %CP-6B volatiles. After PE was ignited, the alkyl chain broken, and a large amount of active radicals $H\cdot$ and $\cdot OH$ generated in the gas phase. These active radicals catalyzed the chain scission of the alkyl chain and accelerate combustion. The amount and intensity of PE/20 %ATH/20 %CP-6B gas phase volatiles

Table 7. Peaks structure of PE/20 %ATH/20 %CP-6B volatiles

Peak	m/z	Structure	Peak	m/z	Structure
1	56		15	156	
2	70		16	166	
3	84		17	168	
4	98		18	170	
5	112		19	194	
6	114		20	182	
7	124		21	184	
8	126		22	194	
9	128		23	182	
10	94		24	212	
11	140		25	194	
12	142		26	210	
13	152		27	184	
14	168		28	252	

were lower than those of PE/40 %ATH. The phosphorus-containing free radicals generated by the decomposition of CP-6B consumed active free radicals. CP-6B reduced the amount of active free radicals in the gas phase and terminated the chain reaction.

Flame Retardant Mechanism

Figure 10 shows the flame retardant model of PE samples. PE consisted of a simple alkyl chain containing only C and H without any flame retardant properties. Therefore, almost no residue formed after pure PE combustion. When ATH was added, Al_2O_3 produced by ATH decomposition covered the surface of the resin by physical accumulation. The physical cover layer had low strength, and the combustion heat and flammable volatiles released by the decomposition of the internal resin easily caused cracks. The Al_2O_3 layer had low heat insulation and oxygen barrier capacity; as such a large amount of ATH should be added to improve the flame retardant efficiency.

Figure 11 shows the decomposition model of CP-6B. After adding CP-6B to PE/ATH, CP-6B decomposed to

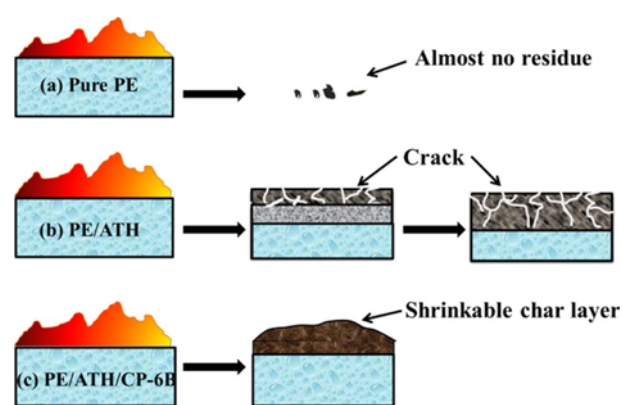


Figure 10. Flame retardant model of ATH and CP-6B, (a) pure PE, (b) PE/ATH, and (c) PE/ATH/CP-6B.

form a network structure and continued to decompose to form a shrinkable carbon layer containing B-O-C [55-56,59]. The continuous char layer produced by the chemical reaction suppressed the generation of cracks and improved

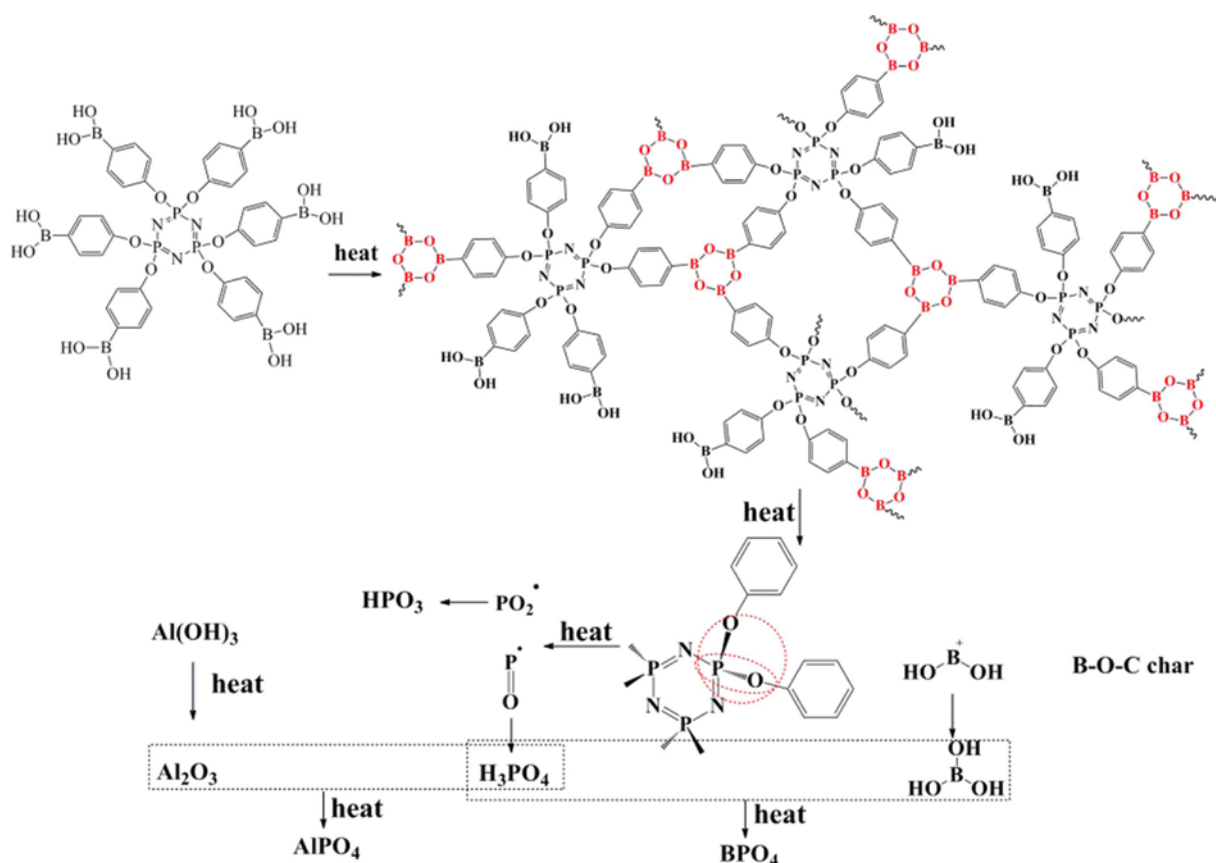


Figure 11. Decomposition model of CP-6B.

the flame retardant efficiency. Al_2O_3 , BPO_4 , and AlPO_4 formed during combustion were dispersed in the char layer, which improved the heat resistance of the char layer. The addition of CP-6B increased the integrity and continues of the char. The barrier effect of char increased, the condensed phase flame retardant efficiency increased. In addition, the decomposition of CP-6B released nitrogen-containing nonflammable gases and phosphorus-containing free radicals, which exerted a gas phase flame retardant mechanism. Therefore, better flame retardant properties were obtained with the synergistic effect of ATH and CP-6B.

Mechanical Property

Table 8 shows the mechanical properties of the PE samples. Pure PE was a typical soft and tough thermoplastic material with high elongation at break and low flexural

modulus. When ATH or CP-6B was added, the stress area of the substrate was smaller than that of pure PE, thereby reducing the tensile strength and elongation at break. With the addition of rigid fillers, the flexural strength and flexural modulus of PE increased. When rigid fillers were added, the interfacial interaction between the PE matrix and the fillers was weakened. When the sample was subjected to stress, more micro cracks were generated in the matrix, which made PE brittle. When 40 wt.% ATH was added, PE/40 %ATH became brittle and ATH had a great damage to the toughness of PE materials. The elongation at break of PE/20 %ATH/20 %CP-6B was 224.1 % of PE/40 %ATH, and the flexural modulus of PE/20 %ATH/20 %CP-6B was 69.0 % of PE/40 %ATH. This finding indicated that CP-6B reduced the effect of ATH on the mechanical properties of PE.

Table 8. Mechanical properties of PE samples

	Tensile strength (MPa)	Elongation at break (%)	Flexural strength (MPa)	Flexural modulus (MPa)
PE	10.3±0.3	681.3±166.0	9.9±1.1	251.9±37.0
PE/40 %ATH	9.4±0.5	13.7±0.7	14.4±0.7	599.7±62.9
PE/20 %ATH/20 %CP-6B	7.7±0.4	30.7±4.0	11.6±0.4	414.0±57.8

Conclusion

ATH was used as a flame retardant for PE due to its low cost and non-toxicity. However, ATH had low flame retardant efficiency and required high amounts to be added, which impaired the mechanical properties of PE. CP-6B containing phosphorus, nitrogen, and boron were selected to improve the flame retardancy of PE/ATH. ATH/CP-6B decomposed nonflammable gases and formed a protective layer. ATH/CP-6B exhibited good synergistic effects. When 20 wt.% ATH and 20 wt.% CP-6B were added, PE/20 %ATH/20 %CP-6B had higher flame retardancy than PE/40 % ATH. CP-6B improved the flame retardant efficiency of PE/ATH and reduced the damage of ATH to the mechanical properties of PE. PE/20 %ATH/20 %CP-6B had good flame retardant properties and mechanical properties.

Acknowledgements

This research was financially supported by the NSFC (Grant Nos. 20774031 and 21074039), the Natural Science Foundation of Guangdong (Grant Nos. 2014A030313241, 2014B090901068, and 2016A010103003).

Electronic Supplementary Material (ESM) The online version of this article (doi: 10.1007/s12221-021-9385-6) contains supplementary material, which is available to authorized users.

References

1. J. Mosnáček, A. A. Basfar, T. M. Shukri, and M. A. Bahattab, *Polym. J.*, **40**, 460 (2008).
2. Y. Liu, D. Y. Wang, J. S. Wang, Y. P. Song, and Y. Z. Wang, *Polym. Adv. Technol.*, **19**, 1566 (2008).
3. X. Li and B. Yang, *J. Therm. Anal. Calorim.*, **122**, 359 (2015).
4. T. M. Shukri, J. Mosnáček, A. A. Basfar, M. A. Bahattab, P. Noireaux, and A. Courdreuse, *J. Appl. Polym. Sci.*, **109**, 167 (2008).
5. M. Masoomi, R. Bagheri, L. Ahmadkhanbeigi, and M. Asgari, *J. Appl. Polym. Sci.*, **131**, 40452 (2014).
6. H. D. Lu, Y. Hu, L. Yang, Z. Z. Wang, Z. Y. Chen, and W. C. Fan, *Macromol. Mater. Eng.*, **289**, 984 (2004).
7. Z. H. Cao, Y. Zhang, P. G. Song, Y. Z. Cai, Q. Guo, Z. P. Fang, and M. Peng, *J. Anal. Appl. Pyrolysis*, **92**, 339 (2011).
8. S. B. Nie, S. H. Qi, M. S. He, and B. X. Li, *J. Therm. Anal. Calorim.*, **114**, 581 (2013).
9. L. P. Li, W. Guo, and C. G. Guo, *Wood Sci. Technol.*, **51**, 493 (2017).
10. L. Ye, P. Ding, M. Zhang, and B. J. Qu, *J. Appl. Polym. Sci.*, **107**, 3694 (2008).
11. G. B. Huang, B. C. Zhu, and H. B. Shi, *J. Appl. Polym. Sci.*, **121**, 1285 (2011).
12. Y. Altun, M. Doğan, and E. Bayramlı, *Eur. J. Wood Prod.*, **74**, 851 (2016).
13. Y. Altun, M. Doğan, and E. Bayramlı, *Fire Mater.*, **40**, 697 (2016).
14. J. Zhao, C. L. Deng, S. L. Du, L. Chen, C. Deng, and Y. Z. Wang, *J. Appl. Polym. Sci.*, **131**, 40065 (2014).
15. Z. P. Wu, Y. C. Hu, and W. G. Shu, *J. Vinyl Addit. Technol.*, **15**, 260 (2010).
16. K. L. Tan, X. S. Chen, B. S. Yan, Y. Z. Lu, and C. X. Li, *J. Appl. Polym. Sci.*, **123**, 3495 (2012).
17. Y. Zhang, X. N. Li, Z. H. Cao, Z. P. Fang, T. R. Hull, and A. A. Stec, *Ind. Eng. Chem. Res.*, **54**, 3247 (2015).
18. S. B. Nie, M. X. Zhang, S. J. Yuan, G. L. Dai, N. N. Hong, L. Song, Y. Hu, and X. L. Liu, *J. Therm. Anal. Calorim.*, **109**, 999 (2012).
19. W. P. Song, W. Zhang, Y. G. Li, H. J. Ma, T. Lin, C. F. Lu, J. Q. Nie, G. C. Yang, and Z. X. Chen, *Fire Mater.*, **43**, 685 (2019).
20. M. Lounisa, S. Lecontea, C. Roussellea, L. P. Belzuncesb, V. Desauzieresc, J. M. Lopez-Cuestac, J. M. Juliend, D. Guenote, and D. Bourgeoisf, *J. Hazard. Mater.*, **366**, 556 (2019).
21. C. H. Chen, C. H. Lin, J. M. Hon, M. W. Wang, and T. Y. Juang, *Polymer*, **154**, 35 (2018).
22. M. Y. Hu, K. K. Xiong, J. R. Li, X. B. Jing, and P. H. Zhao, *Fiber. Polym.*, **20**, 1794 (2019).
23. M. J. Xu, K. Ma, D. W. Jiang, J. X. Zhang, M. Zhao, X. K. Guo, Q. Shao, E. Wujcik, B. Li, and Z. H. Guo, *Polymer*, **146**, 63 (2018).
24. Y. L. Wang, Z. P. Li, Y. Y. Li, J. Y. Wang, X. Liu, T. Y. Song, X. M. Yang, and J. W. Hao, *ACS Appl. Mater. Interfaces*, **10**, 10490 (2018).
25. G. Choo, I. S. Lee, and J. E. Oh, *J. Hazard. Mater.*, **371**, 175 (2019).
26. C. K. Chen, X. L. Zhao, C. L. Shi, and J. Chen, *J. Mater. Sci.*, **53**, 6053 (2018).
27. E. R. Vargas, S. S. Valdes, O. P. Tabla, S. C. Gutie´rrez, J. M. Nonell, L. F. Valle, A. L. León, and R. L. Acosta, *J. Appl. Polym. Sci.*, **123**, 1125 (2012).
28. Z. H. Chang, F. Guo, J. F. Chen, J. H. Yu, and G. Q. Wang, *Polym. Degrad. Stabil.*, **92**, 1204 (2007).
29. S. Zhou, M. Ning, X. F. Wang, Z. J. Yan, D. F. Guo, Q. He, Y. P. Zhang, S. K. She, and Y. Hu, *J. Therm. Anal. Calorim.*, **119**, 167 (2015).
30. C. M. Feng, M. Y. Liang, J. L. Jiang, Y. K. Zhang, J. G. Huang, and H. B. Liu, *J. Appl. Polym. Sci.*, **133**, 43950 (2016).
31. S. M. Liu, J. Y. Huang, Z. J. Jiang, C. Zhang, J. Q. Zhao, and J. Chen, *J. Appl. Polym. Sci.*, **117**, 3370 (2010).
32. Y. J. Kwon, D. K. Kim, W. N. Kim, B. G. Cho, S. M. Hong, and C. M. Koo, *J. Appl. Polym. Sci.*, **124**, 2814 (2012).
33. F. I. Beltrán-Ramírez, L. F. Ramos-deValle, E. Ramírez-Vargas, S. Sánchez-Valdes, A. B. Espinoza-Martínez, J. G.

- Martínez-Colunga, O. S. Rodríguez-Fernandez, E. N. Cabrera-Alvarez, and M. L. López-Quintanilla, *J. Nanomater.*, **2014**, 969184 (2014).
34. S. T. Bee, A. Hassan, C. T. Ratnam, T. T. Tee, and L. T. Sin, *Nucl. Instr. Meth. Phys. Res. B*, **299**, 42 (2013).
35. D. D. Yang, Y. Hu, H. T. Li, L. Song, H. P. Xu, and B. Li, *J. Therm. Anal. Calorim.*, **119**, 619 (2015).
36. S. Q. Chen, B. S. Sun, G. B. Huang, H. C. Guo, and S. Q. Wang, *J. Vinyl Addit. Technol.*, **19**, 285 (2013).
37. C. Kaynak and E. Ibibikcan, *J. Fire Sci.*, **32**, 121 (2014).
38. E. Ibibikcan and C. Kaynak, *J. Fire Sci.*, **32**, 99 (2014).
39. H. L. Gao, S. Hu, H. C. Han, and J. Zhang, *J. Appl. Polym. Sci.*, **122**, 3263 (2011).
40. Z. Katančić, L. K. Krehula, A. P. Siročić, V. Grozdanić, and Z. H. Murgić, *J. Comp. Mater.*, **48**, 3771 (2014).
41. X. J. Kong, S. M. Liu, and J. Q. Zhang, *J. Cent. South Univ. Technol.*, **15**, 779 (2008).
42. M. A. Bahattab, J. Mosnáček, A. A. Basfar, and T. M. Shukri, *Polym. Bull.*, **64**, 569 (2010).
43. N. A. Isitman and C. Kaynak, *J. Fire Sci.*, **31**, 73 (2013).
44. R. K. Jian, Y. F. Ai, L. Xia, L. J. Zhao, and H. B. Zhao, *J. Hazard. Mater.*, **371**, 529 (2019).
45. Y. Miyake, M. Tokumura, Q. Wang, T. Amagai, Y. Takegawa, Y. Yamagishi, S. Ogo, K. Kume, T. Kobayashi, S. Takasu, K. Ogawa, and K. Kannan, *Environ. Sci. Technol. Lett.*, **5**, 448 (2018).
46. G. Yang, W. H. Wu, Y. H. Wang, Y. H. Jiao, L. Y. Lu, H. Q. Qu, and X. Y. Qin, *J. Hazard. Mater.*, **366**, 78 (2019).
47. G. M. Zhou, K. Liu, Y. C. Fan, M. Q. Yuan, B. F. Liu, W. Liu, F. F. Shi, Y. Y. Liu, W. Chen, J. Lopez, D. Zhuo, J. Zhao, Y. Tsao, X. Y. Huang, Q. F. Zhang, and Y. Cui, *ACS Cent. Sci.*, **4**, 260 (2018).
48. Y. Z. Feng, X. W. Li, X. Y. Zhao, Y. S. Ye, X. P. Zhou, H. Liu, C. T. Liu, and X. L. Xie, *ACS Appl. Mater. Interfaces*, **10**, 21628 (2018).
49. K. P. Chen, C. R. Tian, S. E. Liang, X. L. Zhao, and X. L. Wang, *Polym. Degrad. Stabil.*, **150**, 105 (2018).
50. S. Y. Xia, Z. Y. Zhang, Y. Leng, B. Li, and M. J. Xu, *J. Anal. Appl. Pyrol.*, **134**, 632 (2018).
51. N. J. Wu, G. L. Fu, Y. Yang, M. F. Xia, H. Yun, and Q. G. Wang, *J. Hazard. Mater.*, **363**, 1 (2019).
52. B. Zhao, D. Y. Liu, W. J. Liang, F. Li, J. S. Wang, and Y. Q. Liu, *J. Anal. Appl. Pyrol.*, **124**, 247 (2017).
53. H. Y. Ding, K. Huang, S. H. Li, L. Xu, J. L. Xia, and M. Li, *J. Anal. Appl. Pyrol.*, **128**, 102 (2017).
54. S. L. Qiu, C. Ma, X. Wang, X. Zhou, X. M. Feng, R. K. K. Yuen, and Y. Hu, *J. Hazard. Mater.*, **344**, 839 (2018).
55. L. H. Ai, S. S. Chen, J. M. Zeng, P. Liu, W. S. Liu, Y. H. Pan, and D. F. Liu, *Polym. Degrad. Stabil.*, **155**, 250 (2018).
56. T. Zhang, W. S. Liu, M. X. Wang, P. Liu, Y. H. Pan, and D. F. Liu, *Polym. Degrad. Stabil.*, **130**, 257 (2016).
57. Z. S. Xu, Z. Y. Chu, and L. Yan, *J. Therm. Anal. Calorim.*, **133**, 1241 (2018).
58. S. Yang, Q. X. Zhang, and Y. F. Hu, *Polym. Degrad. Stabil.*, **133**, 358 (2016).
59. A. B. Morgan, J. L. Jurs, and J. M. Tour, *J. Appl. Polym. Sci.*, **76**, 1257 (2000).